MAGNETIC STRUCTURE AT THE SURFACE OF A FeZrB ALLOY

M. Pavúk, M. Miglierini and J. Sitek

Institute of Nuclear and Physical Engineering, Slovak University of Technology in Bratislava, Ilkovičova 3, 812 19 Bratislava, Slovak Republic
E-mail: milan.pavuk@stuba.sk

Received 10 May 2013; accepted 14 May 2013

1. Introduction

The alloy studied belongs to the group of nanocrystalline soft magnetic materials called NANOPERM [1]. Alloys of this group have the general composition Fe-*M*-B-(Cu) where *M* denotes a transition metal (such as Zr, Hf, Nb, Ta, and Mo). The most common method of their preparation is by controlled annealing of the initially amorphous alloys. The amorphous precursors are produced by rapid quenching of a melt.

Nanocrystalline alloys have a unique two-phase structure composed of crystalline and amorphous residual phase [2]. The crystalline phase consists of α-Fe grains which are randomly oriented in the residual amorphous phase. The overall representation of the grains in the amorphous phase can be regulated by a proper choice of the temperature and time of annealing [3]. Nanocrystalline grains are responsible for excellent soft magnetic properties [4, 5], and at the same time they stabilize the structure against temperature changes [6].

Magnetic domain structure reflects the behaviour of magnetization. In coarse-grained materials, the size of domains is proportional to the grain sizes. Each grain has its own domain structure. The domain character is determined largely by the crystallographic orientation of surface crystallites [7]. In nanocrystalline materials, however, the domains with their sizes extend over a large number of grains. The domain character is here determined largely by residual anisotropies [7-9].

The aim of this work was to examine two structural states of the $^{57}Fe_{90}Zr_7B_3$ alloy from the point of view of their domain structure. As the method for obtaining the image of a domain structure we used the magnetic force microscopy (MFM). Its advantage is that besides the image of a domain structure, it also records the image of topography. Another advantage is the high spatial resolution. From both of these advantages, one can benefit in the study of nanocrystalline alloys. Nevertheless, the use of MFM in the study of nanocrystalline materials is so far only rare [10-14]. Additional structural characterization was obtained by the help of Conversion Electron Mössbauer Spectrometry (CEMS).

2. Experimental Details

Alloy with the composition of $^{57}Fe_{90}Zr_7B_3$ was produced by planar-flow-casting on a copper wheel. The width of the 21 μm thick ribbons was 1 mm. Structural state of the alloy after production will be referred to as "as-quenched". The alloy was subsequently annealed at 480 °C in an external magnetic field of 652 mT oriented parallel to the length of the ribbon.

The topography of the surface and magnetic force gradients in its vicinity were obtained by Dimension Edge atomic force microscope (Veeco Instruments Inc., USA) from the air (shiny) sides of the ribbons. The measurements were carried out at room temperature. We used a probe with the model name MESP from Veeco Company. Each measured sample of the ribbon was under a force microscope rotated so that the scanning direction was perpendicular to the ribbon length, i.e. the direction of the ribbon preparation. All presented images are oriented with their vertical sides parallel with the ribbon length.

CEMS was performed with a constant acceleration driver equipped with a ^{57}Co(Rh) radiation source. The surface features of the investigated ribbons were scanned to the depth of about 200 nm at room temperature. In order to obtain an enhanced CEMS signal, the alloys were prepared from iron enriched to about 63 % to the stable isotope ^{57}Fe.

3. Results and Discussion

In the as-quenched state, the $^{57}Fe_{90}Zr_7B_3$ alloy is preferentially paramagnetic as demonstrated by a pronounced central Mössbauer broadened doublet in Fig. 1a, *wheel side*. Traces of the doublet can be seen also at the *air side*. At this side of the ribbon, noticeable surface crystallization occurs that was triggered by the production process. The six-line patterns (grey colour) in Fig. 1 correspond to signals from bcc-Fe nanocrystals.

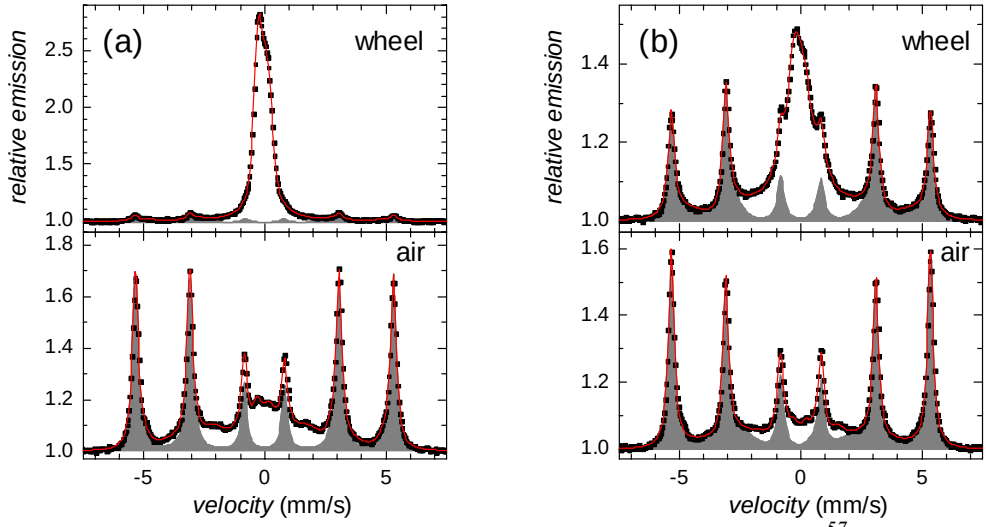

Fig. 1: *CEMS spectra taken from the as-quenched (a) and annealed (b) $^{57}Fe_{90}Zr_7B_3$ ribbon.*

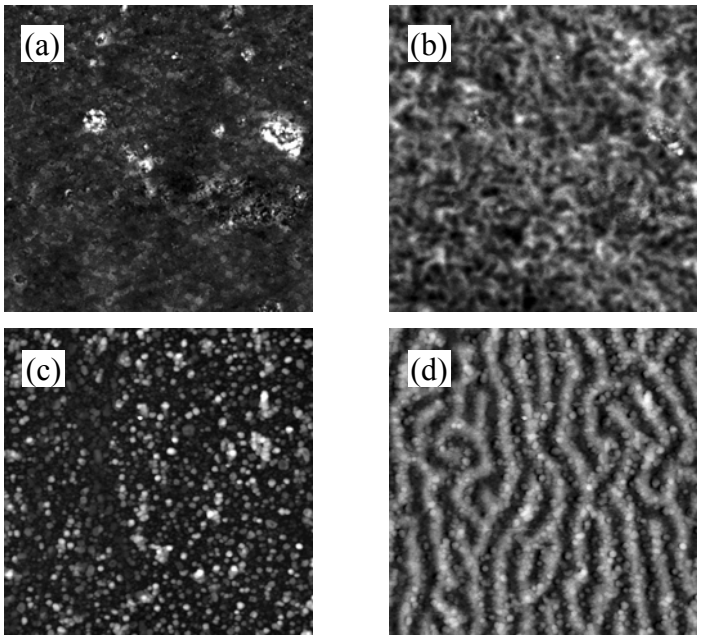

Fig. 2: *Topography (a, c) and phase-domain structure images (b, d) of the as-quenched (a, b) and annealed (c, d) $^{57}Fe_{90}Zr_7B_3$ ribbon. The size of the scanned areas is 10 ×10 μm^2. Both phase images were recorded at a distance of 100 nm from the surface.*

After annealing, the progress of crystallization is well documented in Fig. 1b by an increase of the grey six-line components that represent the bulk as well as surfaces of ferromagnetic bcc-Fe nanograins that have emerged from the originally paramagnetic residual amorphous matrix. The latter exhibits still a doublet-like character especially at the wheel side of the ribbon. This is an indication of non-magnetic states of the resonance atoms in the residual amorphous matrix.

Nanograins that are located at the surfaces of the ribbons are visualised by topography AFM images in Fig. 2a, c while the corresponding phase sensitive MFM images in Fig. 2b, d show the observed domain structures. The latter is rather chaotic in the as-quenched alloy (Fig. 2b). After annealing, a distinguished magnetic order is seen in Fig. 2d. The domains are preferentially oriented along the length of the ribbon. This suggests that during the ribbon preparation, geometrically driven magneto-elastic anisotropy is introduced by the external magnetic field. A stripe pattern is repeated with a period of 0.9 μm, as calculated by Power Spectral Density analyses.

The protrusions in topography of the annealed alloy in Fig. 2c have an average height of 58 nm. If we refine the scanning scale, tiny features that cover almost the complete surface can be also seen in the topography of the as-quenched alloy (Fig. 3a). Their average height is ca. 3 nm and accounting for the corresponding CEMS spectrum in Fig. 1c they can be assigned to bcc-Fe nanocrystalline grains. At this resolution, areas in MFM image have shown up in Fig. 3b where even some magnetic arrangement is observed on a very short-range distance. The protrusions observed in Fig. 3c correspond to agglomerates of crystalline grains that were formed during the annealing. Their magnetic manifestation is seen in Fig. 3d.

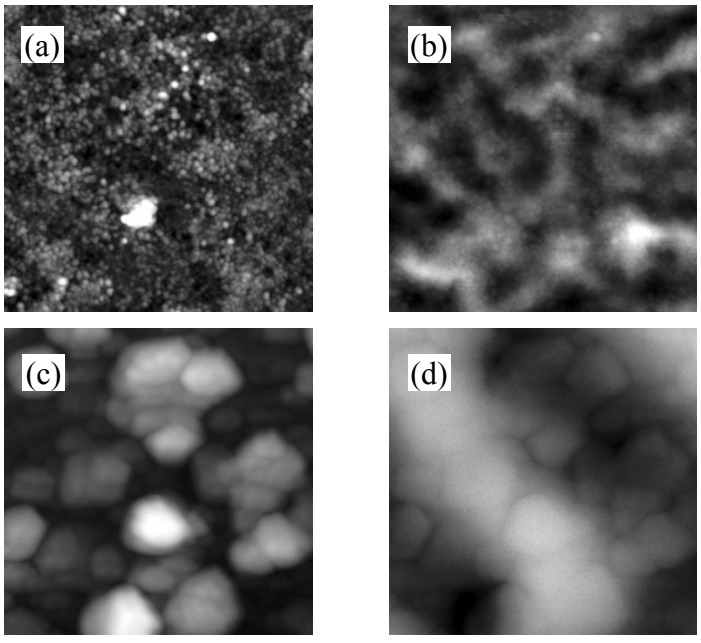

Fig. 3: *Detailed topography (a, c) and phase-domain structure images (b, d) of the as-quenched (a, b) and annealed (c, d) $^{57}Fe_{90}Zr_7B_3$ ribbons. The size of the scanned area is 2 × 2 μm^2 and 1 x 1 μm^2 for (a, b) and (c, d), respectively. The phase images were recorded at a distance of 50 nm (b) and 100 nm (d) from the surface.*

The MFM images of magnetism were measured mainly at a distance of 100 nm from the surface of the ribbon. This distance is sufficient to ensure that short-range forces would not affect the scanning tip. Nevertheless, strong magnetic interactions from topological protrusions are reflected in the phase images as artefacts caused by scanning in the air [15].

4. Conclusions

Surface magnetic structures were investigated in as-quenched and annealed states of a NANOPERM alloy. Topological arrangements were followed by AFM whereas MFM provided phase-domain structure images. Using the results obtained from CEMS that scans the surface regions down to the depth of about 200 nm, presence of bcc-Fe nanocrystallites was revealed already in the as-quenched state. After annealing, their amount was considerably increased. Due to enhanced ferromagnetic exchange interactions among bcc-Fe nanograins, the originally paramagnetic amorphous residual phase was partially polarized. Consequently, well developed magnetic maze domain features were observed. They are preferentially oriented along the length of the ribbon-shaped samples. An almost equally wide stripe patterns are repeated with a period of 0.9 μm. Their character suggests that at the surface the magnetic forces act preferentially perpendicular to the ribbon plane. This is confirmed also by the line intensity ratio of the magnetic sextet in the CEMS spectrum of the annealed alloy taken from the air side of the ribbon. Smaller intensities of the second and the fifth lines indicate that the average magnetization vector tends to turn out of the ribbon plane.

Acknowledgements

This publication is a result of the implementation of the project Centre of Competence in New Materials, Advanced Technologies and Energy, ITMS code 26240220073 which is supported by the Research and Development Operational Programme funded by the European Regional Development Fund. The work was also partially funded by the projects VEGA 1/0286/12 and SK-PL-0032-12.

References:

[1] K. Suzuki, N. Kataoka, A. Inoue and A. Makino: Mater. Trans., JIM, **31**, 743 (1990).
[2] P. Švec, K. Krištiaková, P. Duhaj and D. Janičkovič: Czech. J. Phys., **52**, 145 (2002).
[3] M. Miglierini: J. Non-Cryst. Solids, **354**, 5093 (2008).
[4] G. Herzer: IEEE Trans. Magn., **25**, 3327 (1989); G. Herzer: IEEE Trans. Magn., **26**, 1397 (1990).
[5] G. Herzer: In: *Handbook of Magnetism and Advanced Magnetic Materials*, H. Kronmüller and S. Parkin (eds.), Wiley, 1882 (2007).
[6] G. Herzer: In: *Handbook of Magnetic Materials*, Vol. 10, K. H. J. Buschow (ed.), Elsevier Science, 415 (1997).
[7] R. Schäfer: In: *Nanoscale Magnetic Materials and Applications*, J. P. Liu et al. (eds.), Springer, 275 (2009).
[8] O. Životský, K. Postava, L. Kraus, K. Hrabovská, A. Hendrych and J. Pištora: J. Magn. Magn. Mater., **322**, 1523 (2010).
[9] J. M. Silveyra, G. Vlasák, P. Švec, D. Janičkovič and V. J. Cremaschi: J. Magn. Magn. Mater., **322**, 2797 (2010).
[10] K. Suzuki, D. Wexler, J. M. Cadogan, V. Sahajwalla, A. Inoue and T. Masumoto: Mater. Sci. Eng. A, **226**, 586 (1997).
[11] M. E. Hawley, G. W. Brown, D. J. Thoma, M. A. Willard, D. E. Laughlin and M. E. McHenry: *MRS Proc.*, **577**, 531 (1999).
[12] I. García, N. Iturriza, J. J. del Val, H. Grande, J. A. Pomposo and J. González: J. Magn. Magn. Mater., **322**, 1822 (2010).
[13] M. Miglierini and K. Šafářová: Acta Phys. Pol. A, **118**, 840 (2010).
[14] X. Bao, X. Gao, J. Zhu and S. Zhou: J. Rare Earths, **29**, 939 (2011).
[15] Z. H. Wang, K. Chen, Y. Zhou and B. K. Shen: J. Electron. Sci. Technol. China, **5**, 50 (2007).